PHYSICAL REVIEW D 90, 065018 (2014)

Interaction of photons traversing a slowly varying electromagnetic background

B. King*
School of Computing and Mathematics, Plymouth University, Plymouth PL4 8AA, United Kingdom and Arnold Sommerfeld Center for Theoretical Physics, Ludwig-Maximilians-Universität München, Theresienstraße 37, 80333 München, Germany

P. Böhl† and H. Ruhl‡
Arnold Sommerfeld Center for Theoretical Physics, Ludwig-Maximilians-Universität München, Theresienstraße 37, 80333 München, Germany
(Received 16 June 2014; published 15 September 2014)

When two electromagnetic fields counterpropagate, they are modified due to mutual interaction via the polarized virtual electron-positron states of the vacuum. By studying how photon-photon scattering effects such as birefringence and four-wave mixing evolve as the fields pass through one another, we find a significant increase during overlap when both electromagnetic variants can be nonzero. The results have particular relevance for calculations based on a constant field background.

DOI: 10.1103/PhysRevD.90.065018 PACS numbers: 12.20.-m, 03.50.De, 03.65.Pm, 97.60.Jd

I. INTRODUCTION

That electromagnetic fields can polarize virtual electron-positron pairs of the vacuum has been known since the early pioneering calculations of Sauter [1], Halpern [2], Weisskopf [3] and Heisenberg and Euler [4], later being rederived in the language of quantum electrodynamics by Schwinger [5]. The polarized pairs facilitate the process of photon-photon scattering, which can be broadly split into inelastic processes such as vacuum pair-creation and elastic processes where fermion states do not persist on the mass shell. There are many predicted manifestations of elastic effects. The polarization of scattered photons could be used to verify this phenomenon through birefringence, polarization rotation [6–12] and helicity flipping [9,13]. The propagation direction of scattered photons could also be used and signals of diffraction [14–17] and reflection [18–20] have been calculated. Also in the frequency of scattered photons, signals can occur through the process of four-wave mixing [17,21], photon-splitting [8,22–25] and photon-merging [26–29].

These phenomena are of interest in astrophysics, for example to describe the behavior of magnetized neutron stars [30–37], particularly in astrophysical electromagnetic shocks [38–40] and in high-intensity laser physics [41–43], being searched for in terrestrial experiments [44–46].

When photon wavelengths are much longer than the length on which pair creation occurs, photon-photon scattering can be described using an effective theory for interacting electromagnetic fields given by the Heisenberg-Euler Lagrangian. Typically one considers the effect on some weak "probe" field, which can be a single photon, as it passes through a "strong" field. In applications to potential laser experiments, it is the asymptotic state of the probe field which is of primary interest as detection apparatus is necessarily far removed from the interaction region. In simulations of astrophysics in the magnetospheres of neutron stars, one typically calculates the effect on propagating photons in a classical magnetic field, which is taken to vary adiabatically, with the constant-field solution being integrated over macroscopic regions in kinetic equations [30,47].

In the current paper, we focus on the evolution of an oscillating probe field that scatters in a slowly varying strong background, with both fields being described as plane waves. We will often refer to an "overlap" of fields, which is equivalent to the largest amplitude of the two electromagnetic invariants, defined in the following section. Using the Heisenberg-Euler Lagrangian, we will identify a signal of elastic photon-photon scattering that increases with the overlap of the fields and disappears when the overlap tends to zero. Moreover, we will find that this scattered "overlap field" can be much larger than the "asymptotic" scattered field which persists after the probe has passed through the background, particularly for parameters considered in high-intensity laser experiments. The presence of the overlap field implies a difference in the predicted physics when one calculates effects in a forever-constant background compared to those in a constant background evolved adiabatically from the infinite past. Furthermore, the overlap field is neglected whenever an approximation to elastic photon scattering in inhomogeneous fields is made by integrating over forever-constant background scattering rates.

*ben.king@plymouth.ac.uk
†patrick.boehl@physik.uni-muenchen.de
‡hartmut.ruhl@physik.uni-muenchen.de

II. ANALYTICAL METHOD

Let us consider the electromagnetic field to be the sum of a weak probe and strong background field

$$F^{\mu\nu} = F_p^{\mu\nu} + F_s^{\mu\nu}, \tag{1}$$

where F is the Faraday tensor [48] and the subscripts $_p$ and $_s$ pertain, throughout the paper, to the probe and strong fields, respectively. If one defines dimensionless electromagnetic and secular invariants,

$$\mathcal{F} = -F^2/4E_{\mathrm{cr}}^2, \qquad \mathcal{G} = -FF^*/4E_{\mathrm{cr}}^2, \tag{2}$$

$$a = [\sqrt{\mathcal{F}^2 + \mathcal{G}^2} + \mathcal{F}]^{1/2}, \quad b = [\sqrt{\mathcal{F}^2 + \mathcal{G}^2} - \mathcal{F}]^{1/2}, \tag{3}$$

where $F^2 = F^{\mu\nu}F_{\mu\nu}$, $FF^* = F^{\mu\nu}F_{\mu\nu}^*$, giving $\mathcal{G} = \mathbf{E}\cdot\mathbf{B}$ and $\mathcal{F} = (E^2 - B^2)/2$, in which $E^2 = \mathbf{E}\cdot\mathbf{E}$ and electric and magnetic fields $\mathbf{E}$, $\mathbf{B}$ are dimensionless, having been normalized by the critical field strength $E_{\mathrm{cr}} = m^2/e$. We set here and throughout $\hbar = c = 1$. The one-loop effective action in a constant external field is given by the Heisenberg-Euler Lagrangian [5]

$$\mathcal{L}_{\mathrm{HE}} = -\frac{\alpha m^4}{8\pi^2}\int_0^\infty ds\,\frac{\mathrm{e}^{-s}}{s^3}\left[s^2 ab\cot as\coth bs - 1 + \frac{s^2}{3}(a^2 - b^2)\right]. \tag{4}$$

As we are interested in the effects on electromagnetic fields and wish to avoid a discussion on pair creation, we perform a weak-field expansion of Eq. (4) for when $E \ll 1$,

$$\mathcal{L}_{\mathrm{HE}} = \frac{m^4}{\alpha}\sum_{n=1}^{\infty}\mathcal{L}_n, \tag{5}$$

$$\begin{aligned}
\mathcal{L}_1 &= \frac{\mu_1}{4\pi}[(E^2 - B^2)^2 + 7(\mathbf{E}\cdot\mathbf{B})^2] \\
\mathcal{L}_2 &= \frac{\mu_2}{4\pi}(E^2 - B^2)[2(E^2 - B^2)^2 + 13(\mathbf{E}\cdot\mathbf{B})^2], \\
\mathcal{L}_3 &= \frac{\mu_3}{4\pi}[3(E^2 - B^2)^4 + 22(E^2 - B^2)^2(\mathbf{E}\cdot\mathbf{B})^2 \\
&\quad + 19(\mathbf{E}\cdot\mathbf{B})^4],
\end{aligned} \tag{6}$$

where $\mu_1 = \alpha/90\pi$, $\mu_2 = \alpha/315\pi$, $\mu_3 = 4\alpha/945\pi$ (the fine-structure constant occurs in the denominator in the Lagrange densities Eq. (6) due to rewriting fields in terms of the critical field). The term $\mathcal{L}_n$ describes the effective scattering of $2n$ photons and we will restrict ourselves to the leading-order effects of $\mathcal{L}_1$ corresponding to effective four-photon scattering or the "box diagram," and $\mathcal{L}_2$ corresponding to effective six-photon scattering or the "hexagon diagram," as demonstrated in Fig. 1. It has been shown that in the low-frequency limit $\omega/m \ll 1$, a direct calculation of four-photon scattering agrees with the leading-order term in the above weak-field expansion [49]. A further and more restrictive condition can be placed on the frequencies we consider, when we demand that the work performed by the external field over the reduced Compton wavelength is less than the electron rest energy $\omega/mE \ll 1$. Applying the Euler-Lagrange equations to $\mathcal{L} = \mathcal{L}_{\mathrm{MW}} + \mathcal{L}_{\mathrm{HE}}$, where $\mathcal{L}_{\mathrm{MW}} = m^4(E^2 - B^2)/8\pi\alpha$ leads to the classical Maxwell equations, one arrives at a wave equation modified by vacuum polarization,

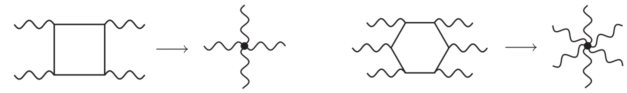

FIG. 1. The Heisenberg-Euler Lagrangian contains effective vertices for classical electromagnetic fields interacting via the quantum effects described by the four-photon scattering box diagram and six-photon scattering hexagon diagram.

$$\Box\mathbf{E} = \mathbf{T}[\mathbf{E}, \mathbf{B}], \tag{7}$$

where we have defined a source term,

$$\mathbf{T} = 4\pi[\nabla\wedge\partial_t\mathbf{M} + \partial_t^2\mathbf{P} - \nabla(\nabla\cdot\mathbf{P})], \tag{8}$$

for dimensionless magnetization $\mathbf{M} = (\alpha/m^4)\partial\mathcal{L}_{\mathrm{HE}}/\partial\mathbf{B}$ and polarization $\mathbf{P} = (\alpha/m^4)\partial\mathcal{L}_{\mathrm{HE}}/\partial\mathbf{E}$. To simplify the discussion, let us consider the probe and strong fields to counterpropagate with normalized wave vectors $\hat{\mathbf{k}}_p = (0, 0, 1)$, $\hat{\mathbf{k}}_s = (0, 0, -1)$ and calculate scattering along the axis of symmetry. This effectively reduces the system to one spatial and one temporal dimension. An interesting consequence of this is that the charge density, given by $\nabla\cdot\mathbf{P}$, disappears. This is due to the electromagnetic field having no component in the direction of inhomogeneity, which is the direction of propagation along the z axis. Therefore, the final term in Eq. (8) can be neglected. Assuming the change in the fields due to scattering is small, we then solve

$$(\partial_t^2 - \partial_z^2)\mathbf{E} = \mathbf{T}[\mathbf{E}^{(0)}], \tag{9}$$

where $\Box\mathbf{E}^{(0)} = \Box\mathbf{B}^{(0)} = 0$ are vacuum solutions to the wave equation, and $\mathbf{B}_j^{(0)} = \hat{\mathbf{k}}_j\wedge\mathbf{E}_j^{(0)}$ for $j \in \{s, p\}$. In particular, we will choose $\mathbf{E}^{(0)}(x^-, x^+) = \mathbf{E}_p(x^-) + \mathbf{E}_s(x^+)$, where $x^\pm = t \pm z$. We wish to solve the scattering problem for when two initially well-separated excitations of the electromagnetic field $\mathbf{E}_p(x^-)$ and $\mathbf{E}_s(x^+)$ that vanish on the boundary ($\lim_{x^\pm\to\pm\infty}\mathbf{E}_{p,s} = 0$) collide at some finite t and z. The solution to Eq. (9) is acquired using

$$\mathbf{E}(t, z) = \mathbf{E}^{(0)}(t, z) + \Delta\mathbf{E}(t, z) \tag{10}$$

$$\Delta\mathbf{E}(t,z) = \int dt'dz' G_{\mathrm{R}}(t-t',z-z')\mathbf{T}[\mathbf{E}^{(0)}(t',z')], \quad (11)$$

where G_{R} is the retarded Green's function for the wave equation in one spatial and one temporal dimension [50]

$$G_{\mathrm{R}}(t,z) = \frac{1}{2}\theta(t)\theta\left(\frac{t}{v}-|z|\right), \quad (12)$$

for propagation speed v, which we will assume to be equal to the speed of light $v=1$ in all calculations in this paper. Applying this method to Eq. (9), we have

$$(\partial_t^2-\partial_z^2)\Delta\mathbf{E} = \mathbf{T}[\mathbf{E}^{(0)}]. \quad (13)$$

The approximation $\mathbf{T}[\mathbf{E}] \approx \mathbf{T}[\mathbf{E}^{(0)}]$ in Eqs. (11) and (13) can be understood by the following argument. Since the source $\mathbf{T}$ contains, to leading order in $E \ll 1$, the cube of electromagnetic fields E^3, the lowest order neglected term is $\sim E^2\Delta E$. An approximation for ΔE can be made by using Eq. (11), which turns out to give $\Delta E \sim \alpha E^3 L_\varphi$ for some phase length L_φ. Therefore, if $\alpha E^2 L_\varphi \ll 1$, the approximation of neglecting the vacuum's influence on the driving fields when calculating vacuum polarization, $\mathbf{T}[\mathbf{E}] \approx \mathbf{T}[\mathbf{E}^{(0)}]$, can be justified. We note the importance not only of field strength, but also of phase length.

Through partial integration in t, the scattered field becomes a sum of forward- (positive z direction) and backward-propagating scattered fields

$$\Delta\mathbf{E}(t,z) = \Delta\overrightarrow{\mathbf{E}}(t,z) + \Delta\overleftarrow{\mathbf{E}}(t,z), \quad (14)$$

where boundary terms can be neglected when the initial overlap of fields is zero, and

$$\Delta\overrightarrow{\mathbf{E}}(t,z) = \int_{-\infty}^{z}\frac{dz'}{2}\mathbf{J}(x^-+z',z') \quad (15)$$

$$\Delta\overleftarrow{\mathbf{E}}(t,z) = \int_{z}^{\infty}\frac{dz'}{2}\mathbf{J}(x^+-z',z'), \quad (16)$$

where $x^\pm = t \pm z$ and $\mathbf{J}$ is the current occurring in Maxwell's equations

$$\mathbf{J}(t,z) = 4\pi[\widehat{\mathbf{k}}_p \wedge \partial_z\mathbf{M}(t,z) + \partial_t\mathbf{P}(t,z)]. \quad (17)$$

The interpretation of $\Delta\overrightarrow{\mathbf{E}}(t,z)$, $\Delta\overleftarrow{\mathbf{E}}(t,z)$ as the forward- and backward-scattered field, respectively, can be seen more clearly by rewriting Eqs. (15) and (16) in light cone coordinates (where the substitution $y=2(z'-z)$ has been made):

$$\Delta\overrightarrow{\mathbf{E}}(x^-,x^+) = \int_{-\infty}^{0}\frac{dy}{4}\mathbf{J}(x^-,x^++y) \quad (18)$$

$$\Delta\overleftarrow{\mathbf{E}}(x^-,x^+) = \int_{0}^{\infty}\frac{dy}{4}\mathbf{J}(x^--y,x^+). \quad (19)$$

Therefore $\Delta\overrightarrow{\mathbf{E}}(t,z)$ remains constant on the probe-field light cone, (x^- constant i.e. forward-scattered) and $\Delta\overleftarrow{\mathbf{E}}(t,z)$ on the strong field light cone (x^+ constant i.e. backward-scattered).

A. Overlap and asymptotic field

To make clearer what is happening, we calculate by way of example, part of the forward-scattered field Eq. (15) arising from the second term in the current Eq. (17) using Eqs. (10) and (11). The polarization is

$$\mathbf{P}[\mathbf{E}] = \frac{\mu_1}{2\pi}[2(E^2-B^2)\mathbf{E} + 7(\mathbf{E}\cdot\mathbf{B})\mathbf{B}], \quad (20)$$

where we recall we consider $\mathbf{P}[\mathbf{E}^{(0)}]$ and since $\mathbf{E}^{(0)}(t,z) = \mathbf{E}_s(x^+) + \mathbf{E}_p(x^-)$ and similarly for the magnetic field, which are both plane waves, we see different combinations of powers of E_s and E_p will occur in $\mathbf{P}$. For brevity, let us focus on terms proportional to the probe field squared. Then the corresponding part of the scattered field is

$$\boldsymbol{\varepsilon}\int_{-\infty}^{z}\frac{dz'}{2}\partial_{t'}(E_p^2E_s), \quad (21)$$

where $\boldsymbol{\varepsilon}$ is the polarization vector that absorbs all other constants in this example, $E_p = E_p(t'-z')$, $E_s = E_s(t'+z')$ and the derivative is evaluated at $t' = x^- + z'$, which becomes

$$-\boldsymbol{\varepsilon}\int_{-\infty}^{z}\frac{dz'}{2}\partial_{z'}(E_p^2)E_s + \boldsymbol{\varepsilon}\int_{-\infty}^{z}\frac{dz'}{2}E_p^2\partial_{z'}(E_s). \quad (22)$$

Equation (22) is the *asymptotic* plus the *overlap* field, respectively. To elaborate these labels, we can use that the derivatives are evaluated on the light cone of the probe field so that Eq. (22) becomes

$$\tfrac{1}{2}\boldsymbol{\varepsilon}E_p'(x^-)E_p(x^-)\textstyle\int_{-\infty}^{0}dyE_s(x^++y) + \tfrac{1}{2}\boldsymbol{\varepsilon}E_p^2(x^-)E_s(x^+), \quad (23)$$

where $'$ indicates the derivative. For the first term, we see that on the probe light cone (e.g. $x^-=0$), long after the collision in the asymptotic limit $t,z\to\infty$, the term remains (assuming the integration over the strong field is nonvanishing). Therefore we label this the *asymptotic* scattered field. The second term corresponds to a surface term and the strong and probe fields are evaluated on their respective light cones. When the overlap of the fields, or equivalently the amplitude of the field invariants, tends to zero, so does this term and therefore we label this the *overlap* scattered field. We note that if a constant field is adiabatically evolved from the infinite past, the overlap field *is* generated. This should be contrasted with the case of an ever-present constant field, in which the overlap field vanishes identically.

In this example we considered the probe field squared, corresponding to generation of a second harmonic (the frequency of the strong field is taken to be much smaller than that of the probe), also referred to as "photon-merging". A division into overlap and asymptotic scattered fields can be made in each combination of powers of strong and probe fields that occur in the interaction.

To investigate these ideas, we will choose the probe and strong fields in this paper to be of the form

$$\mathbf{E}_p(\varphi_p) = \boldsymbol{\varepsilon}_p \mathcal{E}_p \mathrm{e}^{-(\frac{\varphi_p}{\Phi_p})^2} \cos\varphi_p \tag{24}$$

$$\mathbf{E}_s(\varphi_s) = \boldsymbol{\varepsilon}_s \mathcal{E}_s \mathrm{e}^{-(\frac{\varphi_s}{\Phi_s})^2}, \tag{25}$$

where $\Phi_j = \omega_j \tau_j$ and $\varphi_j = k_j^\mu x_\mu$ for $j \in \{s, p\}$, $\boldsymbol{\varepsilon}_p \cdot \boldsymbol{\varepsilon}_p = \boldsymbol{\varepsilon}_s \cdot \boldsymbol{\varepsilon}_s = 1$ and we are interested in the case $\omega_p \tau_s \gg 1$.

III. NUMERICAL METHOD

The numerical solution of the nonlinear Maxwell equations following from the sum of classical and Heisenberg-Euler Lagrangians is based on the PCMOL (pseudo characteristic method of lines) [51], matrix inversion and the CVODE ODE-Solver from SUNDIALS (suite of nonlinear and differential/algebraic equation solvers) [52]. Since we assume propagation only in the z direction and only transverse polarizations, the resulting equations of motion can be written in matrix form,

$$(\mathbb{1}_4 + \mathbf{A})\partial_t \mathbf{f} + (\mathbf{Q} + \mathbf{B})\partial_z \mathbf{f} = 0, \tag{26}$$

where $\mathbf{f} = (E_x, E_y, B_x, B_y)^T$, $\mathbb{1}_4 = \mathrm{diag}(1,1,1,1)$ is the identity matrix in four dimensions, $\mathbf{Q} = \mathrm{adiag}(1,-1,-1,1)$ is an antidiagonal matrix and $\mathbf{A} = (a_{ij})$ and $\mathbf{B} = (b_{ij})$ are the nonlinear corrections resulting from Eq. (5) with $a_{ij} = b_{ij} = 0$ for $i > 2$. For the weak field expansion $\mathcal{L}_1$ ($\mathcal{L}_2$), the components are quadratic (fourth order) polynomials of the field components.

Let us first consider the linear case with $\mathbf{A} = \mathbf{B} = \mathbf{0}$. In the PCMOL, one uses the diagonalizability of the matrix $\mathbf{Q}$, which means one can find a basis $\mathbf{u} \coloneqq \mathbf{P}\mathbf{f}$ such that $\mathbf{\Lambda} = \mathbf{P}\mathbf{Q}\mathbf{P}^{-1} = \mathrm{diag}(-1,-1,1,1)$ is diagonal with real eigenvalues:

$$\mathbf{P} = \frac{1}{\sqrt{2}}\begin{pmatrix} -1 & 0 & 0 & 1 \\ 0 & 1 & 1 & 0 \\ 1 & 0 & 0 & 1 \\ 0 & -1 & 1 & 0 \end{pmatrix} \qquad \mathbf{u} \coloneqq \mathbf{P}\mathbf{f} = \frac{1}{\sqrt{2}}\begin{pmatrix} B_y - E_x \\ E_y + B_x \\ E_x + B_y \\ B_x - E_y \end{pmatrix}. \tag{27}$$

The new set of equations is given by

$$\partial_t \mathbf{u} + \mathbf{\Lambda}\partial_z \mathbf{u} = 0. \tag{28}$$

The eigenvalues are called the characteristic speeds and the positive (negative) sign corresponds to a component propagating in the positive (negative) z direction. The system, which is taken to be of a length of 320 μm, is discretized in space using $N = 2 \times 10^5$ points. The four-dimensional vector $\mathbf{u}$ can then be mapped onto a $4N$-dimensional one, $\mathbf{u} = (\ldots u_4^{i-1} u_1^i u_2^i u_3^i u_4^i u_1^{i+1} \ldots)$, where $0 < i \leq N$ labels the grid point. The spatial derivatives of the components u_j^i are approximated with upwind-biased finite differences determined by the sign of the characteristic speed. This is done using fourth-order stencils [53], where the values of the derivative near the boundary are also approximated with fourth-order accuracy using grid points only inside the simulation box. Since the derivatives at one point are calculated with the field values at the specific and surrounding points, the action of the derivative can be written as a matrix multiplication: $\partial_z \mathbf{u} \approx \mathbf{D}\mathbf{u}$, where $\mathbf{D}$ is a $4N \times 4N$ matrix. In the PCMOL, the equations are now transformed back to the original basis $\mathbf{f}$, but the system is solved in $\mathbf{u}$, which is completely equivalent. This has the advantage of automatically implementing open boundary conditions due to the upwind character in the single components. The electric and magnetic fields are then obtained by applying $\mathbf{P}^{-1}$ for output at each grid point.

We now consider the nonlinear case. To bring the system to an ODE form $\mathbf{u}'(t) = f(\mathbf{u}, t)$ (f is called the "right-hand-side function," the $'$ denotes the time derivative), we need to invert the matrix $(\mathbb{1}_4 + \mathbf{A})$. Since $\mathbf{A}$ is a local operator of the field components, it is only necessary to consider the inversion for each single grid point. We rewrite $\mathbf{A}$ as $\mathbf{A} = \mathbf{M}\mathbf{N}$ with

$$\mathbf{M} = \begin{pmatrix} 1 & 0 \\ 0 & 1 \\ 0 & 0 \\ 0 & 0 \end{pmatrix}, \qquad \mathbf{N} = \begin{pmatrix} a_{11} & a_{12} & a_{13} & a_{14} \\ a_{21} & a_{22} & a_{23} & a_{24} \end{pmatrix} \tag{29}$$

and apply the Woodbury formula [54],

$$(\mathbb{1}_4 + \mathbf{A})^{-1} = \mathbb{1}_4 - \mathbf{M}(\mathbb{1}_2 + \mathbf{N}\mathbf{M})^{-1}\mathbf{N}, \tag{30}$$

to reduce the inversion of the 4×4-matrix $(\mathbb{1}_4 + \mathbf{A})$ to one of the 2×2 matrix,

$$(\mathbb{1}_2 + \mathbf{N}\mathbf{M}) = \begin{pmatrix} 1 + a_{11} & a_{12} \\ a_{21} & 1 + a_{22} \end{pmatrix}, \tag{31}$$

which is performed at each evaluation of the right-hand-side function f via an LU factorization. Since our method employs a weak field expansion, we expect only small corrections from the nonlinearities $\mathbf{A}$ and $\mathbf{B}$, such that the matrix $(\mathbb{1}_4 + \mathbf{A})^{-1}(\mathbf{Q} + \mathbf{B})$ has similar spectral properties (i.e. the same signs of the eigenvalues) as $\mathbf{Q}$. Therefore we use the same biased differencing as in the linear case. The system is now solved using the parallel, extended-precision version of CVODE, where the nonlinear right-hand-side function is given by

$$f(\mathbf{u},t) = -\mathbf{P}(\mathbb{1}_4 + \mathbf{A})^{-1}(\mathbf{Q}+\mathbf{B})\mathbf{P}^{-1}\mathbf{D}\mathbf{u}. \tag{32}$$

$\mathbf{P}(\mathbb{1}_4 + \mathbf{A})^{-1}(\mathbf{Q}+\mathbf{B})\mathbf{P}^{-1}$ is now a block-diagonal $4N \times 4N$ matrix with 4×4 blocks acting on each grid point, as explained above. We use the provided Adams-Moulton methods and the functional iteration to solve the corresponding linear system of equations. The signals are analyzed using a spatial Fourier transform in Wolfram MATHEMATICA [55], and the frequency components are filtered under the assumption $\omega = |\mathbf{k}|$ and transformed back to spatial coordinates. To analyze the dc component, we subtract the analytical expression of the strong pulse from the signal.

IV. COMPETING VACUUM PROCESSES

For clarity, we consider each frequency component of the scattered field separately and neglect the change in frequency due to the background frequency scale $1/\tau_s \ll \omega_p$. To leading order in $\mathcal{E}_s, \mathcal{E}_p \ll 1$, the scattered field can be written as

$$\Delta\mathbf{E} = \sum_{l=1}^{\infty} \mathcal{E}_p^l \mathrm{e}^{-l(\frac{\varphi_p}{\Phi_p})^2}[\mathbf{C}_l \sin l\varphi_p + \tilde{\mathbf{C}}_l \cos l\varphi_p] + \mathcal{E}_p^2[\mathbf{C}_0 + \tilde{\mathbf{C}}_0]. \tag{33}$$

In Eq. (33) we note that the scattered field is written as a sum over harmonics of the probe field. Each higher harmonic involves a higher power of $\mathcal{E}_p \ll 1$ so in general higher harmonics are less likely in this regime. For each harmonic we then note two spacetime-dependent vector terms with coefficients $\mathbf{C}_l$ and $\tilde{\mathbf{C}}_l$. The $\mathbf{C}_l$ terms are out of phase with the probe field and form the asymptotic field whereas the $\tilde{\mathbf{C}}_l$ terms are in phase with the probe field and correspond to the overlap field. Although we neglect processes of a higher order than four- and six-photon scattering in the current analysis, they can be calculated straightforwardly using the method used here. We highlight the fact that $\lim_{\mathcal{E}_s\to 0}\mathbf{C}_l = \lim_{\mathcal{E}_s\to 0}\tilde{\mathbf{C}}_l = \lim_{\mathcal{E}_s\to 0}\mathbf{C}_0 = \lim_{\mathcal{E}_s\to 0}\tilde{\mathbf{C}}_0 = 0$, showing that $\Delta\mathbf{E}$ vanishes in the limit where the strong or probe field is absent. In the following we comment on the first few harmonics.

A. Fundamental harmonic

If the scattered field is much weaker than the probe, it can be described by analogy with a modified refractive index, $1+\delta n$, $\delta n \ll 1$. The probe field light cone then becomes $\varphi_p = \omega_p[t/(1+\delta n) - z]$. Expanding $\cos\varphi_p$ in δn, the leading-order scattered field is in antiphase with the probe field, so this effect should be entirely covered by the asymptotic field in our analysis. For the current scenario we find

$$\mathbf{C}_1 = -\mu_1 \boldsymbol{\varepsilon}_{s,1}\mathcal{E}_s^2 \frac{\omega_p\tau_s\sqrt{\pi}}{\sqrt{2}} \frac{1+\mathrm{erf}(\sqrt{2}\varphi_s/\Phi_s)}{2} \tag{34}$$

$$\tilde{\mathbf{C}}_1 = -\mu_1 \boldsymbol{\varepsilon}_{s,1} E_s^2(\varphi_s), \tag{35}$$

where the polarization of the scattered field is given by

$$\boldsymbol{\varepsilon}_{s,1} = c_{1,1}\boldsymbol{\varepsilon}_s + c_{1,2}\hat{\mathbf{k}}_s \wedge \boldsymbol{\varepsilon}_s, \tag{36}$$

with coefficients

$$c_{1,1} = 4\boldsymbol{\varepsilon}_s\cdot\boldsymbol{\varepsilon}_p(1 - \hat{\mathbf{k}}_s\cdot\hat{\mathbf{k}}_p), \tag{37}$$

$$c_{1,2} = 7(\boldsymbol{\varepsilon}_s\cdot\hat{\mathbf{k}}_p\wedge\boldsymbol{\varepsilon}_p + \boldsymbol{\varepsilon}_p\cdot\hat{\mathbf{k}}_s\wedge\boldsymbol{\varepsilon}_s). \tag{38}$$

In particular, we notice that when $\hat{\mathbf{k}}_p = \hat{\mathbf{k}}_s$, $c_{1,1} = c_{1,2} = 0$ and vacuum polarization effects disappear, as they must in a single plane wave background [5]. The polarization vector of the scattered field in all harmonics will be a function of these coefficients, so we highlight that $c_{1,1}$ originates from evaluating $\mathcal{F}_{ps} = -F_p^{\mu\nu}F_{s\mu\nu}/4E_{\mathrm{cr}}^2$ and $c_{1,2}$ from evaluating $\mathcal{G}_{ps} = -F_p^{\mu\nu}F_{s\mu\nu}^*/4E_{\mathrm{cr}}^2$. Therefore, a considerable simplification occurs when $\boldsymbol{\varepsilon}_s \| \boldsymbol{\varepsilon}_p$ implying $c_{1,2}\to 0$ or when $\boldsymbol{\varepsilon}_s \perp \boldsymbol{\varepsilon}_p$ implying $c_{1,1} = 0$. A consistency check of Eqs. (34) and (35) can be performed by calculating the implied altered dispersion relation for the probe field. We note that the well-known modified refractive index for $\hat{\mathbf{k}}_p = -\hat{\mathbf{k}}_s$ in a constant background is given by [6]

$$\delta n(\varphi_s) = \frac{2\alpha E_s^2(\varphi_s)}{45\pi}[4(\boldsymbol{\varepsilon}_p\cdot\boldsymbol{\varepsilon}_s)^2 + 7(\boldsymbol{\varepsilon}_p\wedge\boldsymbol{\varepsilon}_s)^2]. \tag{39}$$

If the corresponding phase difference $\delta\varphi_p$ is calculated by integrating Eq. (39) over the shape of E_s in the following way,

$$\delta\varphi_p(z') = \omega_p\int_{-\infty}^{z'} dz\, \delta n(\varphi_s)|_{t=z-x^{-\prime}}, \tag{40}$$

then the asymptotic field and Eq. (34) can be recovered exactly.

The presence of the overlap field in the fundamental harmonic cannot be described by a modified index of refraction. If the background is wider than several probe wavelengths ($\omega_p\tau_s \gg 1$), then the amplitude of the overlap field is much smaller than that of the asymptotic in the fundamental harmonic. Both parts of the scattered field have the same polarization as the probe in this case.

B. Second harmonic

The strongest contribution to the scattered field with double the frequency of the probe originates from four- and six-photon scattering. We find

$$\mathbf{C}_2 = -\mu_2 \boldsymbol{\varepsilon}_{s,2} \mathcal{E}_s^3 \frac{\omega_p \tau_s \sqrt{\pi}}{\sqrt{3}} \frac{1+\mathrm{erf}(\sqrt{3}\varphi_s/\Phi_s)}{2} \tag{41}$$

$$\tilde{\mathbf{C}}_2 = -\frac{\mu_1}{2} \boldsymbol{\varepsilon}_{p,1} E_s(\varphi_s) - \frac{\mu_2}{2} \boldsymbol{\varepsilon}_{s,2} E_s^3(\varphi_s), \tag{42}$$

where

$$\boldsymbol{\varepsilon}_{p,1} = c_{1,1}\boldsymbol{\varepsilon}_p + c_{1,2}\widehat{\mathbf{k}}_p \wedge \boldsymbol{\varepsilon}_p \tag{43}$$

$$\boldsymbol{\varepsilon}_{s,2} = c_{2,1}\boldsymbol{\varepsilon}_s + c_{2,2}\widehat{\mathbf{k}}_s \wedge \boldsymbol{\varepsilon}_s, \tag{44}$$

with $c_{2,1} = 3c_{1,1}^2/2 + 13c_{1,2}^2/49$ and $c_{2,2} = 13c_{1,1}c_{1,2}/14$. In one temporal and one spatial dimension, merging of two photons via four-photon scattering in a strictly constant background is suppressed for kinematical reasons. However, when the background contains some inhomogeneity, the second harmonic *can* be generated. This is also the case when a constant background is adiabatically evolved from the infinite past. Since the second-harmonic overlap field is of order α^2 and the asymptotic field of order α^3, there is a range of parameters for which the overlap field dominates. Let us define the gauge- and relativistically invariant parameter ζ,

$$\zeta = \int_{-\infty}^{\infty} d\varphi_s \zeta(\varphi_s), \tag{45}$$

where $\zeta(\varphi_s) = [\chi(\varphi_s)]^2/\eta$, $\chi = \sqrt{|k_p F_s|^2}/m$ is the so-called quantum nonlinearity parameter [56] and $\eta = k_p k_s/m^2$. For the current scenario, $\zeta = \mathcal{E}_s^2 \omega_p \tau_s \sqrt{2\pi}$, and by comparing Eqs. (41) and (42), we note that when $\zeta \ll 1$, the overlap field can dominate. The evolution of the scattered field is illustrated in Fig. 2, and directly compared with the position of the probe and strong fields. In Fig. 3, the maximum of the amplitude of the simulated second-harmonic signal is plotted and the evolution for the asymptotic and overlap fields compared. In the second harmonic, the rate of change of the overlap field is proportional to the gradient of the background. In Fig. 3 we observe that the maximum of the amplitude of the overlap field initially increases to an overall maximum when the probe and strong fields most overlap, after which the second harmonic is further generated field but phase-shifted by π and destructively interferes with the already present second harmonic field.

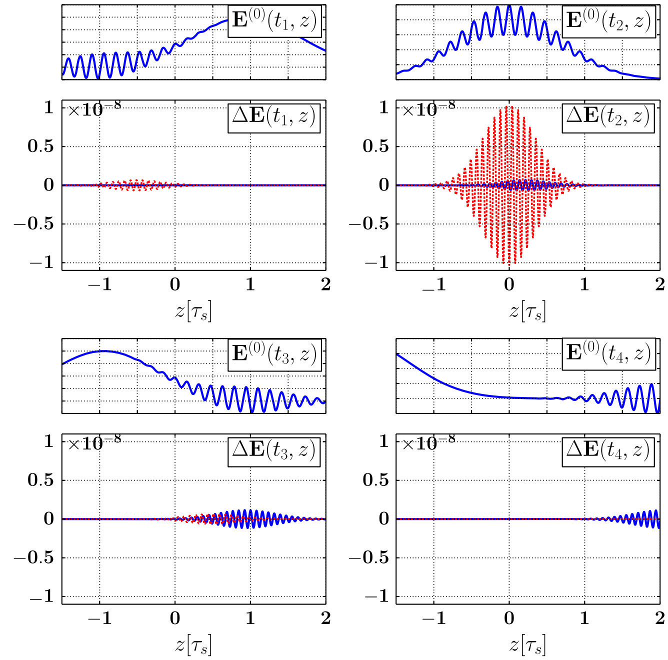

FIG. 2 (color online). The smaller panels plot snapshots of the total electric field above the larger panels showing the corresponding state of the scattered overlap (red dashed) and asymptotic (blue solid) second harmonic field at times $t_4 > t_3 > t_2 > t_1$. The electric fields are in units of the probe field amplitude, $\mathcal{E}_p$.

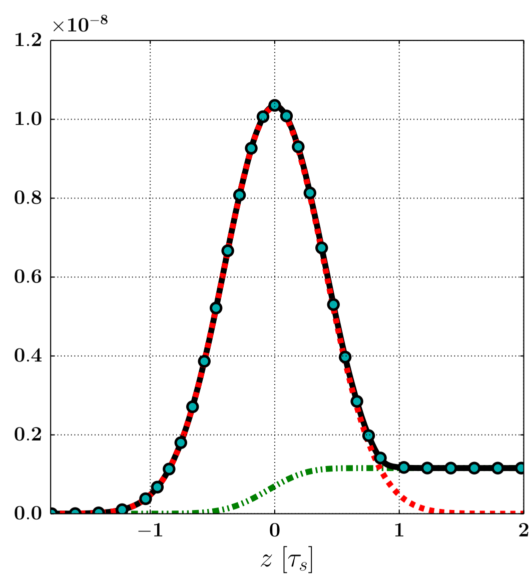

FIG. 3 (color online). The second harmonic overlap field (dashed line) generated in four-photon scattering can dominate the asymptotic field (dot-dashed line) generated in six-photon scattering. Agreement is also shown between simulation (points) and theory (solid line) for $\mathcal{E}_s = 0.02$, $\mathcal{E}_p = 0.005$, $\lambda_p = 2000$ nm, $\tau_s = 6.4\lambda_p$ and $\tau_p = 5\lambda_p$, where the field is in units of the probe amplitude, $\mathcal{E}_p$.

C. Higher harmonics

In the presence of some background inhomogeneity, a given harmonic is generated in the overlap field at one order in α lower than in the scattered field. For example, in one spatial and one temporal dimension, no asymptotic third harmonic signal is generated from the hexagon diagram, but an overlap signal *is* permitted. We find

$$\tilde{\mathbf{C}}_3 = -\frac{\mu_2}{4}\boldsymbol{\varepsilon}_{p,2}E_s^2(\varphi_s), \tag{46}$$

where $\boldsymbol{\varepsilon}_{p,2} = c_{2,1}\boldsymbol{\varepsilon}_p + c_{2,2}\widehat{\mathbf{k}}_p \wedge \boldsymbol{\varepsilon}_p$ and the leading-order term in $\mathbf{C}_3$ can be found by calculating the octagon diagram in the weak-field Heisenberg-Euler expansion using Eq. (6).

Although the overlap and asymptotic fields have different spacetime dependencies, we find that the polarization selection rules for higher harmonic generation are identical. In particular,

$$l\gamma_\parallel \to \gamma'_\parallel; \qquad 2l\gamma_\perp \to \gamma'_\parallel \qquad (2l-1)\gamma_\perp \to \gamma'_\perp, \tag{47}$$

where $\gamma_\parallel$ corresponds to a probe photon obeying $\boldsymbol{\varepsilon}_p \wedge \boldsymbol{\varepsilon}_s = \mathbf{0}$, $\gamma_\perp$ to $\boldsymbol{\varepsilon}_p \cdot \boldsymbol{\varepsilon}_s = 0$, $l \in \mathbb{N}^+$ and γ' is the photon generated through scattering. Therefore odd harmonics exhibit a slightly different polarization behavior and in particular admit a photon-merging cascade in the $\perp$ component. However, since this requires a minimum of three photons to merge, it is presumably only of relevance when the probe photon density is very high or path length very long. Another feature of this mechanism is that probe photons that are in a superposition of linear polarizations *can* access the $\gamma_\perp + \gamma_\perp \to \gamma'_\perp$ channel, but only once. This can be seen by the coefficient of the outgoing $\perp$ channel depending on the overlap of probe photon $\perp$ and $\parallel$ components [e.g. $c_{2,2}$ in Eq. (44)]. After being scattered once, the merged photons are then confined to residing in a polarization eigenmode thereafter.

The lowest-order nontrivial effect of the polarized vacuum on probe photons is a modification of the index of refraction [Eq. (39)] leading to $k^2 \neq 0$. We note that taking this nontrivial dispersion into account, more harmonics can be generated for a given-order diagram in which photons are no longer described by null fields as $F^2 \neq 0$. In particular, the signal must no longer be in harmonics of the incoming field. We will postpone analysis of this particular problem, which requires longer path lengths, for a future publication.

D. Zeroth harmonic

With the zeroth harmonic, dc component, or rectification, we are referring to a signal with the low frequency $\approx 1/\tau_s \ll \omega_p$ of the background. One probe photon is absorbed by and one photon emitted from the polarized vacuum pairs, leaving a photon of the frequency associated

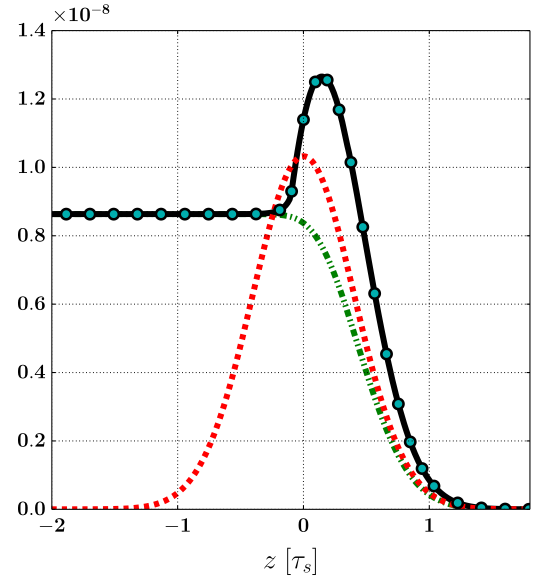

FIG. 4 (color online). Both asymptotic (dot-dashed line) and overlap (dashed line) signals for frequency down-conversion originate from four-photon scattering. The leading-order asymptotic signal is due to the change in background due to interaction with the probe. Theory (solid line) and simulation (points) agree and show a backwards-propagating signal. The parameters are the same as in Fig. 3 and fields in units of the probe amplitude, $\mathcal{E}_p$.

with the background. From momentum conservation, the scattered field has a momentum vector in the backwards direction. We find

$$\mathbf{C}_0 = -\mu_1\boldsymbol{\varepsilon}_{p,1}\mathcal{E}_s\sqrt{\frac{\pi}{2}}\frac{\tau_p}{\tau_s}\frac{\varphi_s}{\Phi_s}\mathrm{e}^{-(\frac{\varphi_s}{\Phi_s})^2}\frac{1+\mathrm{erf}(\sqrt{2}\varphi_p/\Phi_p)}{2}$$
$$\tilde{\mathbf{C}}_0 = -\frac{1}{2}\mu_1\boldsymbol{\varepsilon}_{p,1}E_s(\varphi_s)\mathrm{e}^{-2(\frac{\varphi_p}{\Phi_p})^2}. \tag{48}$$

Emission in the backwards direction is demonstrated in Fig. 4, and contrasts with the photon-merging behavior shown in Fig. 3. Moreover, when the background varies, both asymptotic and overlap signal are generated in four-photon scattering. The polarization of the dc component is then parallel to the strong field $\gamma_\parallel$.

Frequency down-conversion can also produce non-dc components, for example in $\gamma + \gamma \to \gamma + \gamma'$, for probe photons γ, the scattered photon γ' is at the fundamental frequency. However, the more photons that participate, the smaller the effect when $\mathcal{E}_p \ll 1$. We stress the difference of frequency down-conversion from photon splitting, as in the current case, no photon quantum is being split into quanta of lower energy.

V. DISCUSSION

Our results suggest that when one approximates photon-photon scattering in spacetime-varying fields by assuming that scattering is at each instant equivalent to that in a strictly constant background, important physics is missed. We have seen how this even arises when a photon propagates through a quasiconstant background, due to the photon-photon interaction current involving derivatives of combinations of fields. When this current is integrated over, part of the scattered field is generated by a surface term that depends on the state of the background in the photon's past. Therefore it can occur that changes in the background strength, even when over distances much larger than the photon wavelength, can lead to a significant contribution to the rate of photon-photon scattering. In particular, the predicted evolution of the total scattered field is different for a strictly constant background compared to a constant background that has been adiabatically evolved from the infinite past. This could have potential implications for effects calculated in the overlap of probe and strong fields that rely on the instantaneously constant background approximation, such as the so-called "vacuum resonance" [57,58] in strongly magnetized pulsars, which could be searched for in a program similar to the GEMS mission [59].

The intense magnetic field of certain neutron stars offers an excellent possibility to study strong-field quantum electrodynamical effects using polarization measurements of emitted photons [59,60]. The process of photon-splitting has been hypothesized to be of particular importance in the magnetospheres of neutron stars. Here we compare the density of photons (number per unit volume) that split $\rho_{\gamma\to 2\gamma'}$ with those that merge $\rho_{2\gamma\to\gamma'}$ in a quasiconstant magnetic field of strength B. We repeated the calculation leading to Eqs. (41) and (42), first taking the limit $\tau_{p,s}\to\infty$ and setting the background electric field to zero but allowing a background field strength difference ΔB over the seed photons' history, defining $\Delta = \Delta B/B$. We then find

$$\tilde{\rho}_{2\gamma\to\gamma'} = 2\alpha^3\left[\frac{11\pm 3}{180\pi}\right]^2 B^2\Delta^2\frac{\omega}{m}(\rho\pi\lambda\!\!\!^{-}{}^3)\rho \qquad (49)$$

$$\rho_{2\gamma\to\gamma'} = 8\alpha^3\left[\frac{37\mp 11}{315\pi}\right]^2 B^2\zeta^2\frac{\omega}{m}(\rho\pi\lambda\!\!\!^{-}{}^3)\rho \qquad (50)$$

$$\rho_{\gamma\to 2\gamma'} = \frac{\alpha^3}{10}\left[\frac{19}{315\pi}\right]^2\frac{L}{\lambda\!\!\!^{-}}B^6\left(\frac{\omega}{m}\right)^5\rho, \qquad (51)$$

where $\tilde{\rho}_{2\gamma\to\gamma'}$ and $\rho_{2\gamma\to\gamma'}$ refer to merging in the overlap and asymptotic fields, respectively, ρ is the density of seed photons with frequency ω, L is propagation distance of the seed photon, $\zeta = B^2\omega L$ and $\pm$ refer to seed photon polarization being perpendicular or parallel to that of the external field and we have adapted the rate for photon-splitting from [61]. Photon-splitting requires dispersion to be taken into account and has a strong dependence on the frequency being split $\sim(\omega/m)^5$, whereas photon merging requires a high density of photons such that the number of seeds in a cylindrical volume of radius $\lambda\!\!\!^{-}$ around the photon's trajectory is not too small. Although a full comparison is beyond the scope of this paper, if one notes that in a photon gas at temperature T the density of photons with energies $\in[\omega,\omega+\delta\omega]$, $\delta\omega/\omega\ll 1$ is of the order $\rho\sim\omega^2\delta\omega[\exp(\omega/T)-1]^{-1}$, then the ratio of second harmonic generation to photon splitting is of the dependency

$$\frac{\rho_{2\gamma\to\gamma'}}{\rho_{\gamma\to 2\gamma'}}\sim\frac{L\delta\omega}{e^{\omega/T}-1} \qquad (52)$$

$$\frac{\tilde{\rho}_{2\gamma\to\gamma'}}{\rho_{\gamma\to 2\gamma'}}\sim\left(\frac{m}{\omega}\frac{\Delta}{B^2}\right)^2\frac{\lambda\!\!\!^{-}}{L}\frac{\delta\omega}{m}\frac{1}{e^{\omega/T}-1}. \qquad (53)$$

When is harmonic generation more prevalent than electron-positron pair creation in a strongly magnetized thermal photon gas? If the number density of pairs created in photon-photon collisions is $\rho_{2\gamma\to e^+e^-}$ and pairs created through photon decay in a background constant magnetic field $\rho_{\gamma\to e^+e^-}$ then

$$\rho_{2\gamma\to e^+e^-}\sim 2\frac{1}{\lambda\!\!\!^{-}{}^3}\frac{L}{\lambda\!\!\!^{-}}\left(\frac{\alpha}{2\pi}\right)^2\left(\frac{T}{m}\right)^3 e^{-\frac{2m}{T}} \qquad (54)$$

$$\rho_{\gamma\to e^+e^-}\sim\frac{3^{3/4}\alpha}{4\sqrt{2}\pi^{3/2}}\frac{1}{\lambda\!\!\!^{-}{}^3}\frac{L}{\lambda\!\!\!^{-}}\left(\frac{T}{m}\right)^2\delta^{1/4}e^{-\frac{4}{\sqrt{3\delta}}}, \qquad (55)$$

for $T/m\ll 1$ and $\delta = TB/2m\ll 1$ where the pair-creation densities were adapted from [62,63] for a constant magnetic background. In order to calculate the total density of merged photons created in a photon gas, we would have to extend our calculation to include merging of photons with different wave vectors and integrate the double-photon rate over a double Bose-Einstein distribution. However, from Eqs. (54) and (55) we already note that for $T/m\ll 1$, pair creation is exponentially suppressed whereas photon merging (and splitting) are perturbative in T/m. Since $T/m\sim 10^{-4}$ for strongly magnetized neutron stars [34], one could pose the question whether harmonic generation, along with photon splitting, can be an important factor in the evolution of these stellar objects.

We close by noting that only the asymptotic photon merging signal is of relevance to laser physics, and then only when the laser background occurs to an even power and hence contains a slowly-varying component. This occurs in six-photon scattering if pulses collide at an angle which is proportional to $\mathcal{E}_p^3\mathcal{E}_s^2$, or in eight-photon scattering which is proportional to $\mathcal{E}_p^3\mathcal{E}_s^4$ and considering that $\mathcal{E}_{p,s}\ll 1$, these signals are greatly suppressed. This suppression can be potentially overcome by using an ultrashort strong laser pulse and looking off-axis for emitted photons [17] using more than two laser frequencies and off-axis beams [21], or using a charged projectile such as a proton [64,65].

VI. CONCLUSION

We have shown that when an oscillating probe field propagates through a background field with some inhomogeneity, a source of photon-photon scattering appears when the two fields overlap and the field invariants are nonvanishing. This "overlap field" disappears when the overlap of the two fields tends to zero and is distinct from the "asymptotic field" that persists after scattering has taken place. Moreover, the overlap field permits high harmonic generation for a specific harmonic at an order of the fine structure constant lower than in the asymptotic field. By integrating the weak-field expansion of the Heisenberg-Euler Lagrangian using the Green's function for the wave equation in one spatial and one temporal dimension, we compared the nature of the overlap and asymptotic fields and identified a suitable nonlinearity parameter. We have highlighted the potential importance of this effect in astrophysical environments by calculating the density of merged photons and contrasted this with the density of photons split and density of photons seeding pair creation.

ACKNOWLEDGMENTS

B. K. acknowledges the hospitality of H. R. and the Arnold Sommerfeld Center for Theoretical Physics at the Ludwig Maximilians University as well as useful editorial suggestions from T. Heinzl. P. B. acknowledges the very useful advice of A. Hindmarsh during development of the computational simulation. This work was supported by Grant No. DFG, FOR1048, RU633/1-1, by SFB TR18 project B12 and by the Cluster-of-Excellence Munich-Centre for Advanced Photonics (MAP). Plots were generated with MATPLOTLIB [66].

[1] F. Sauter, Z. Phys. **69**, 742 (1931).
[2] O. Halpern, Phys. Rep. **44**, 855 (1934).
[3] V. Weisskopf, Kgl. Danske Videnskab. Selskab, Mat.-fys. Medd. **14**, 6 (1936).
[4] W. Heisenberg and H. Euler, Z. Phys. **98**, 714 (1936).
[5] J. Schwinger, Phys. Rev. **82**, 664 (1951).
[6] R. Baier and P. Breitenlohner, Nuovo Cimento B **47**, 117 (1967).
[7] N. B. Narozhnyĭ, Sov. Phys. JETP **28**, 371 (1969).
[8] S. L. Adler, Ann. Phys. (N.Y.) **67**, 599 (1971).
[9] V. N. Baĭer, A. I. Mil'shteĭn, and V. M. Strakhovenko, Sov. Phys. JETP **42**, 961 (1976).
[10] A. Di Piazza, K. Z. Hatsagortsyan, and C. H. Keitel, Phys. Rev. Lett. **97**, 083603 (2006).
[11] T. Heinzl, B. Liesfeld, K.-U. Amthor, H. Schwoerer, R. Sauerbrey, and A. Wipf, Opt. Commun. **267**, 318 (2006).
[12] B. King, A. Di Piazza, and C. H. Keitel, Phys. Rev. A **82**, 032114 (2010).
[13] V. Dinu, T. Heinzl, A. Ilderton, M. Marklund, and G. Torgrimsson, Phys. Rev. D **89**, 125003 (2014).
[14] B. King, A. D. Piazza, and C. H. Keitel, Nat. Photonics **4**, 92 (2010).
[15] D. Tommasini and H. Michinel, Phys. Rev. A **82**, 011803(R) (2010).
[16] Y. Monden and R. Kodama, Phys. Rev. Lett. **107**, 073602 (2011).
[17] B. King and C. H. Keitel, New J. Phys. **14**, 103002 (2012).
[18] G. Y. Kryuchkyan and K. Z. Hatsagortsyan, Phys. Rev. Lett. **107**, 053604 (2011).
[19] H. Gies, F. Karbstein, and N. Seegert, New J. Phys. **15**, 083002 (2013).
[20] V. Dinu *et al.*, arXiv:1405.7291.
[21] E. Lundström, G. Brodin, J. Lundin, M. Marklund, R. Bingham, J. Collier, J. Mendonça, and P. Norreys, Phys. Rev. Lett. **96**, 083602 (2006).
[22] Z. Bialynicka-Birula and I. Bialynicki-Birula, Phys. Rev. D **2**, 2341 (1970).
[23] I. Affleck and L. Kruglyak, Phys. Rev. Lett. **59**, 1065 (1987).
[24] G. Brodin, M. Marklund, B. Eliasson, and P. K. Shukla, Phys. Rev. Lett. **98**, 125001 (2007).
[25] A. Di Piazza, K. Z. Hatsagortsyan, and C. H. Keitel, Phys. Plasmas **14**, 032102 (2007).
[26] Z. Bialynicka-Birula, Physica (Amsterdam) **2D**, 513 (1981).
[27] A. Di Piazza, K. Z. Hatsagortsyan, and C. H. Keitel, Phys. Rev. D **72** (2005).
[28] A. M. Fedotov, Proc. SPIE Int. Soc. Opt. Eng. **6726**, 67261D (2007).
[29] H. Gies, F. Karbstein, and R. Shaisultanov, arXiv:1406.2972.
[30] M. G. Baring, Astron. Astrophys. **249**, 581 (1991).
[31] A. K. Harding, M. G. Baring, and P. L. Gonthier, Astrophys. J. **476**, 246 (1997).
[32] M. G. Baring and A. K. Harding, Astrophys. J. **547**, 929 (2001).
[33] W. C. G. Ho and D. Lai, Mon. Not. R. Astron. Soc. **338**, 233 (2003).
[34] A. K. Harding and D. Lai, Rep. Prog. Phys. **69**, 2631 (2006).
[35] D. M. Gitman and A. Shabad, Phys. Rev. D **86**, 125028 (2012).
[36] C. Costa, D. Gitman, and A. Shabad, Phys. Rev. D **88**, 085026 (2013).
[37] T. C. Adorno, D. M. Gitman, and A. Shabad, Eur. Phys. J. C **74**, 2838 (2014).
[38] V. V. Zheleznyakov and A. L. Fabrikant, Sov. Phys. JETP **55**, 794 (1982).
[39] J. S. Heyl and L. Hernquist, Phys. Rev. D **58**, 043005 (1998).
[40] J. S. Heyl and L. Hernquist, Phys. Rev. D **59**, 045005 (1999).

[41] M. Marklund and P. K. Shukla, Rev. Mod. Phys. **78**, 591 (2006).

[42] F. Ehlotzky, K. Krajewska, and J. Z. Kamiński, Rep. Prog. Phys. **72**, 046401 (2009).

[43] A. Di Piazza, C. Müller, K. Z. Hatsagortsyan, and C. H. Keitel, Rev. Mod. Phys. **84**, 1177 (2012).

[44] G. Zavattini, U. Gastaldi, R. Pengo, G. Ruoso, F. Della Valle, and E. Milotti, Int. J. Mod. Phys. A **27**, 1260017 (2012).

[45] P. Berceau, M. Fouche, R. Battesti, and C. Rizzo, Phys. Rev. A **85**, 013837 (2012).

[46] T. N. Wistisen and U. I. Uggerhøj, Phys. Rev. D **88**, 053009 (2013).

[47] C. Thompson and R. C. Duncan, Mon. Not. R. Astron. Soc. **275**, 255 (1995).

[48] J. D. Jackson, *Classical Electrodynamics* (Wiley, New York, 1975).

[49] R. Karplus and M. Neuman, Phys. Rev. **80**, 380 (1950).

[50] G. D. Mahan, *Applied Mathematics* (Springer, New York, 2002).

[51] M. B. Carver, J. Comput. Phys. **35**, 57 (1980).

[52] A. C. Hindmarsh, P. N. Brown, K. E. Grant, S. L. Lee, R. Serban, D. E. Shumaker, and C. S. Woodward, ACM Trans. Math. Softw. **31**, 363 (2005).

[53] W. E. Schiesser, *The Numerical Method of Lines Integration of Partial Differential Equations*, Vol. 17 (Academic Press San Diego, 1991).

[54] G. H. Golub and C. F. Van Loan, *Matrix Computations*, Vol. 3 (Johns Hopkins University Press, Baltimore, 2012).

[55] I. Wolfram Research, *Mathematica* (Wolfram Research, Inc., Champaign, Illinois, 2012), version 9.0 ed.

[56] V. I. Ritus, J. Russ. Laser Res. **6**, 497 (1985).

[57] W. C. G. Ho and D. Lai, Mon. Not. R. Astron. Soc. **327**, 1081 (2001).

[58] W. C. G. Ho and D. Lai, Astrophys. J. **607**, 420 (2004).

[59] P. Ghosh *et al.*, arXiv:1301.5514.

[60] R. Taverna *et al.*, arXiv:1311.7500.

[61] V. O. Papanyan and V. I. Ritus, Sov. Phys. JETP **34**, 1195 (1972).

[62] B. King, A. Di Piazza, and H. Gies, Phys. Rev. D **86**, 125007 (2012).

[63] B. King, H. Gies, and A. Di Piazza, Phys. Rev. D **87**, 069905 (2013).

[64] A. Di Piazza, K. Z. Hatsagortsyan, and C. H. Keitel, Phys. Rev. Lett. **100**, 010403 (2008).

[65] A. Di Piazza, K. Z. Hatsagortsyan, and C. H. Keitel, Phys. Rev. A **78**, 062109 (2008).

[66] J. D. Hunter, Comput. Sci. Eng. **9**, 90 (2007).